Reduced order aerodynamic modeling for a large capacity airship

Yuyao Chen[1], Alvaro Sanchez Ruiz[2], and Guillaume Martinat[3]

[1] Master Student, ISAE-ENSMA,86360 Chasseneuil-du-Poitou, France
yuyao.anais.chen@gmail.com
[2] Master Student, ISAE-ENSMA & ETSIAE-UPM,86360 Chasseneuil-du-Poitou, France
[3] Aerodynamics Department Manager of FLYING WHALES, 92150 Suresnes, France
guillaume.martinat@flying-whales.com

Abstract. FLYING WHALES has launched the LCA60T program to develop a Large Capacity Airship with a capacity of 60 tonnes. The aerodynamic model of the LCA60T is integrated into a 1D flight dynamics model while it remains subject to uncertainties under highly unsteady conditions such as incident gusts of wind. But the full model is not realistic to calculate with limited time and cost, so in this paper, a reduced order model of incoming lateral wind on the airship is created. Based on the bibliography, Proper Orthogonal Decomposition (POD) is a good method to project Navier-Stokes equations to obtain the reduced model. To choose the most adaptable POD for 2D,3D model, the comparison of different interpolation functions,inner product, snapshot and classical methods, scalar-POD and POD approaches are conducted. The 2D reduced model is established and able to reconstruct the velocity field with an error of 0.55%.

Keywords: Aerodynamics · Proper Orthogonal Decomposition · Reduced Order Model.

1 Introduction

The company FLYING-WHALES is a French start-up created in 2012 for providing solutions to the French National Forest Office (ONF) to facilitate wood extraction carrying up to 60 tons of wood trunks.This project called LCA60T for Large Capacity Airship 60 Tons is supported by French government for *Transports de Demain* and *La Nouvelle France Industrielle* from 2013. The great advantage of airship is the low cost, hovering, flexibility, ecofriendly and safe without the need of ground infrastructures and payload volume limitation so that the limitation of the physiognomy could be neglected. To optimize the goals of zero-ground infrastructures and maximum the operability and availability of airship for different meteorological, the Flight dynamics need to react to the strong wind by the elevator and rudder to maneuver. The difference between the airplane or elevator is that the airship is lighter-than-air while the others belong to heavy-than-air which means that some parameters neglected for airplane and helicopter need to be considered in airship. As the airship is large enough and the average cruise speed is around 100 km/h, so that the wind effect can be different between the nose and tail. The reality is that the supplementary parameters come from Navier-Stokes equation which means that once the velocity field and pressure field are known, there is no need to consider more terms as all the forces are located at each nodes rather than gravity center that is called Navier-Stokes based model.

But the Navier-Stokes based model is too expensive to achieve : a mesh with 19 million of cells needs 45 hours to calculate in parallel for 12 processors. So that the reduced order model (ROM) method(Atwell and King, 1999; Atwell 2000is inspired by this problematic: to create the reduced order model for airship to decrease the cost and accelerate the simulation to achieve the reaction with real-time.

The criteria for a good reduced order model is to conserve the characteristics and properties, to minimize the error from the original model and to calculate efficiently and robustly. To reach these goals, the method Proper Orthogonal Decomposition (POD) which has been inspired from Galerkin methods by Boris G. Galrkin in 1915 has been widely discussed. Turk, M. and Pentland, A. (1991) adapted the Principle Component Analysis(PCA) which is the same theory with POD to facial recognition in Machine Learning; Barone, M.F. et al. (2009) used it to model fluid structure interaction; Amsallem, D., Cortial, J. and Farhat, C. (2010) adapted it to real-time aeroelastic computation; Poirion F. (2016) applied to non-Gaussian process like wind, sea wave, seismic ground motion; Brunton, S.L. and Noack, B.R. (2015) implement it to the closed-loop turbulence control.

The advantage of Galerkin projection is that the Navier-Stokes equations can be projected onto a low-dimensional function subspace in order to obtain the ordinary differential equation rather than partial differential equation which leads to calculate and predict different flow solutions without recalculating the whole solution for hours with CFD. Lieu, T. and Farhat, C. (2007) shows its capability to predict the aeroelastic behavior of full fighter aircraft with a decent level of accuracy and operate in real-time but with the limitation of one parameter like incidence for example. Amsallem, D., Cortial, J. and Farhat, C. (2010) improved it with arbitrary sets of parameter values.

As the POD method needs to define the inner product for projection in Hilbert space, a lot of researchers discretized the inner product in different ways which mainly depends on the piece-wise function grouped in finite element mass matrix (Morgan, K. and Peraire, J.,1998): Cordier L. and Bergmann M. (2003) chose the piece-wise linear interpolation, and Liberge E. and Hamdouni A.(2010), Chen H. et al. (2013), P.Thomas Jeffrey et al. (2003) used the dataset of velocity field directly without finite element mass matrix. The relation between these methods and the POD theory will be detailed in the Section 2. And Reduced Order Model theory will be introduced in Section 3. Two directions of airship are important:lateral and forward. In this paper, the lateral model is studied. The 2D reduced order model will be detailed in the Section 4 and POD method will be applied to 3D model in section 5 which allows offering the conclusion in Section 6.

2 Proper Orthogonal Decomposition

The aim of POD is to find the subspace by projection which can conserve the largest information represented by largest mean square projection or least square errors. This subspace has also the smallest errors represented by the least squared error between the original field and projected field. In this section, the POD method is introduced following the formulation of Lumley(1967),Sirovich (1987), Bergmann M.(2004) , Liberge, E. and Hamdouni, A. (2010).

2.1 Inner product

To measure the variances and errors, the inner product (.,.) needs to be define in Hilbert space H, in this lecture, H=$L^2(\Omega)$ where the canonical L^2 inner product is defined :

$$(\boldsymbol{u}, \boldsymbol{v}) = \int_{\Omega} \boldsymbol{u}\boldsymbol{v} d\Omega \tag{1}$$

There are more choices of inner product, but with the consideration of the physical explanation for the energy spectrum (Bergmann M.,2004), the canonical inner product is adopted in this report, and it can be discretized in different formula by different interpolation. Cordier L. and Bergmann M. (2003) chose the piece-wise linear interpolation $N_{I_{linear}}(x)$ .Another two possibilities for the interpolation are the piece-wise constant interpolation $N_{I_{constant}}(x)$ and the piece-wise Dirac function $N_{I_{dirac}}(x)$, which is defined by:

$$\int_{\Omega} N_{I_{dirac}}(\boldsymbol{x}) N_{J_{dirac}}(\boldsymbol{x}) d\Omega = \begin{cases} 0, \, ifI \neq J \\ 1, \, ifI = J \end{cases} \tag{2}$$

To make it better to understand, the 1D case is shown in figure 1.

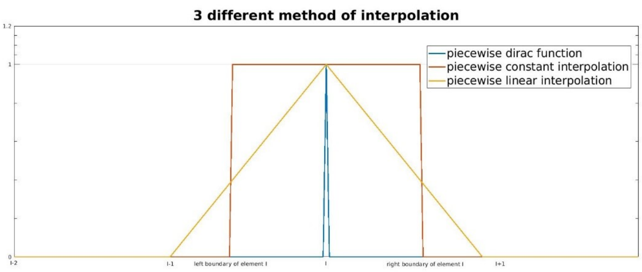

Fig. 1. Three different method of interpolation

Thanks to the interpolation, the velocity can be expressed by the following equation:

$$\boldsymbol{u}(\boldsymbol{x}, t) = \sum_{I=1}^{node} \boldsymbol{u}(I, t) N_I(\boldsymbol{x}) \tag{3}$$

By using the piece-wise Dirac equation, the inner product becomes:

$$(\boldsymbol{u}, \boldsymbol{v}) = \sum_{I=1}^{node} \boldsymbol{u}\left(I, t\right) \boldsymbol{v}\left(I, t\right) \int_{\Omega} N_{I_{dirac}}\left(\boldsymbol{x}\right) N_{I_{dirac}}\left(\boldsymbol{x}\right) d\Omega = \sum_{I=1}^{node} \boldsymbol{u}\left(I, t\right) \boldsymbol{v}\left(I, t\right) \tag{4}$$

While using the piece-wise constant equation, the inner product becomes:

$$\begin{aligned}(\boldsymbol{u},\boldsymbol{v}) &= \sum_{I=1}^{node} \boldsymbol{u}\,(I,t)\,\boldsymbol{v}\,(I,t)\int_{\Omega} N_{I_{constant}}\,(\boldsymbol{x})\,N_{I_{constant}}\,(\boldsymbol{x})\,d\Omega \\ &= \sum_{I=1}^{node} \boldsymbol{u}\,(I,t)\,\boldsymbol{v}\,(I,t)\,dV_I\end{aligned} \tag{5}$$

One advantage of piecewise constant interpolation and Dirac function is its independence of mesh shape and easier way to use without finite element mass matrix $M_{IJ} = (N_I\boldsymbol{x}, N_J\boldsymbol{x})) = \int_{\Omega} N_I\,(\boldsymbol{x})\,N_J\,(\boldsymbol{x})\,d\Omega$. It has the same equation for different types of mesh: triangular, rectangular or even mixed. Moreover the Dirac function is more independent than piecewise constant as it does not need to consider the volume of mesh. So in this paper, the Dirac function is adopted.

A lot of researchers like Liberge E. and Hamdouni A.(2010); Chen H. et al.(2013); P.Thomas Jeffrey et al.(2003); Braud, C. et al.(2004) choose to use the discrete scalar product and consider it separately in different direction x , y, z, for example x direction:

$$(u,v)_x = \sum_{I=1}^{node} u_x(I,t)v_x(I,t) \tag{6}$$

When this method is applied to POD, it is called The scalar-POD,the comparison result of scalar-POD and POD will be shown in Section 4.

2.2 Basis functions and correlation matrix

For the velocity field in $L^2(\Omega)$ with the help of discretization, the finite dimension makes it possible to find finite orthogonal normalized basis functions as shown below:

$$\boldsymbol{u}(\boldsymbol{x},t) = \sum_{m=1}^{node} a^{(m)}(t)\boldsymbol{\phi}^{(m)}(\boldsymbol{x}) \tag{7}$$

The aim of POD is to find the basis functions satisfying:

$$\max_{\boldsymbol{\phi}\in L^2(\Omega)}\left\{\frac{< |(\boldsymbol{u},\boldsymbol{\phi})|^2 >}{\|\boldsymbol{\phi}\|^2}\right\} \tag{8}$$

With normalized basis functions $(\boldsymbol{\phi},\boldsymbol{\phi}) = \|\boldsymbol{\phi}\|^2 = 1$

In fluid dynamics, the dimensionless velocity for example for a controlled cylinder can be presented like:

$$\boldsymbol{U}\,(\boldsymbol{x},t) = \frac{1}{U_0}(\boldsymbol{u}\,(\boldsymbol{x},t) - <\boldsymbol{u}\,(\boldsymbol{x},t)>_t - \gamma\boldsymbol{u_c}\,(\boldsymbol{x},t)) \tag{9}$$

where U_0 inlet velocity, $<\cdots>_t$ time averaged,$\boldsymbol{u_c}\,(\boldsymbol{x},t)$ reference flow field, $\gamma(t)$ control function like rotation velocity. In the following part, the dimensionless unit is used without the influence of the units.

Correlation matrix $\mathcal{R}$ is widely used in order to compare the level of correlation between parameters. The two-point space-time correlation tensor is defined here below :

$$\mathcal{R}(\boldsymbol{x},\boldsymbol{x}') = <\boldsymbol{U}\,(\boldsymbol{x},t)\otimes\boldsymbol{U}\,(\boldsymbol{x}',t)>_t \tag{10}$$

Where $\otimes$ is the dyadic product. The operator $\mathbf{R} : \mathcal{L}^2\,(\Omega) \longrightarrow \mathcal{L}^2\,(\Omega)$ can be defined:

$$\mathbf{R}\;\boldsymbol{\phi}\,(\boldsymbol{x}) = \int_{\Omega}\mathcal{R}\,(\boldsymbol{x},\boldsymbol{x}')\,\boldsymbol{\phi}\,(\boldsymbol{x}')\,d\boldsymbol{x}' \tag{11}$$

as the Riesz and Nagy, 1955; Courant and Hilbert, 1953 proved that the maximum equation 8 is equal to :

$$\mathbf{R}\;\boldsymbol{\phi} = \lambda\boldsymbol{\phi} \tag{12}$$

Solving equation 12, this method is called classical POD. This method is adapted to the case where the mesh is small and the time is large because the spatial correlation matrix will use more space to save while the time information can be calculated by average. For the big mesh and small time, the spatial correlation matrix will take more than two hours to solve. So that another method called snapshot will replace the spatial correlation matrix by temporal in this report as the mesh is large enough. To change the spatial correlation matrix to a temporal one, the equation 13 insert in equation 12,

$$\boldsymbol{\phi}\left(\boldsymbol{x}\right)=\sum_{k=1}^{N_t} b(t_k)\boldsymbol{U}\left(\boldsymbol{x},t_k\right) \tag{13}$$

Which is proved to exist solution by Holmes et al.(1996), then equation 12 becomes :

$$\sum_{k=1}^{N_t}\frac{1}{N_t}\left(\sum_{I=1}^{node}\boldsymbol{U}\left(I,t_i\right)\boldsymbol{U}\left(I,t_k\right)\left(\int_{\Omega}N_I(\boldsymbol{x})N_I(\boldsymbol{x})d\boldsymbol{x}\right)\right)b(t_k)=\lambda b(t_i) \tag{14}$$

The temporal correlation matrix C with size $N_t * N_t$ is defined with piece-wise Dirac function:

$$C_{ik}=\frac{1}{N_t}\left(\sum_{I=1}^{node}\boldsymbol{U}\left(I,t_i\right)\boldsymbol{U}\left(I,t_k\right)\right)=\frac{1}{N_t}\left(D^TD\right) \tag{15}$$

where D is the dataset of velocity field

$$D=[D_xD_yD_z]' \quad Where \quad D_x=\begin{bmatrix} U_x\left(1,t_1\right) & \dots & U_x\left(1,t_{N_t}\right) \\ \dots & \dots & \dots \\ U_x\left(node,t_1\right) & \dots & U_x\left(node,t_{N_t}\right)\end{bmatrix} \tag{16}$$

And the equation 14 can be reformulated as:

$$C\ \mathcal{B}_i=\ \lambda\ \mathcal{B}_i \tag{17}$$

where $\mathcal{B}_i=[b_i(t_1)\dots b_i(t_{N_t})]'$, $\mathcal{B}=\left[\mathcal{B}_1\ \dots\ \mathcal{B}_{N_t}\right]$

By solving the eigen problems, the eigen value and eigen vectors could be obtained, its relations with basis function and velocity :

$$\boldsymbol{\phi}^{(m)}\left(\boldsymbol{x}\right)=\sqrt{N_t\lambda_m}\boldsymbol{\varphi}^{(m)}\left(\boldsymbol{x}\right) \tag{18}$$

where λ_m is the mode eigen value, $\boldsymbol{\varphi}^{(m)}\left(\boldsymbol{x}\right)$ is the m mode eigen vector.

$$\boldsymbol{U}\left(\boldsymbol{x},t_i\right)=\sqrt{N_t}\sum_{m=1}^{N_t}\sqrt{\lambda_m}\boldsymbol{\varphi}^{(m)}(\boldsymbol{x})b_m(t_i)=\sum_{m=1}^{N_t}r^{(m)}\left(t_i\right)\boldsymbol{\varphi}^{(m)}\left(\boldsymbol{x}\right) \tag{19}$$

where $r^{(m)}\left(t_i\right)=\sqrt{N_t\lambda_m}\ b_m(t_i)$

Compared with the random process $X(t,\omega)$ through the Karhunen-Love expansion which is the same methodology as above(Porion, F.,2016) which ensures the result.

$$X(\omega,t)\ =\ \sum_{m\geq 1}\sqrt{\lambda_m}\varphi^{(m)}(\omega)b_m(t) \tag{20}$$

2.3 Number of truncation

The N_t dimension-subspace is too large to operate, thus the smaller subspace will be decided by the number of truncation N_{POD} which is also the dimension of this subspace. The truncated velocity field can be decomposed by basis functions:

$$\boldsymbol{U}\left(\boldsymbol{x},t_i\right)_{truncated}=\sum_{m=1}^{N_{POD}}r^{(m)}\left(t_i\right)\boldsymbol{\varphi}^{(m)}\left(\boldsymbol{x}\right) \tag{21}$$

One of the criteria to choose the number of truncation is the relative information content :

$$\varepsilon=\frac{\sum_{m=1}^{N_{POD}}\lambda_m}{\sum_{m\geq 1}\lambda_m} \tag{22}$$

Which is related to the average mean fluctuation energy E of velocity over the domain:

$$E=\frac{1}{V}\int_{\Omega}\frac{1}{2}<\boldsymbol{U}(\boldsymbol{x},t_i)^2>_t d\Omega=\frac{1}{V}\sum_{m=1}^{N_t}\frac{1}{2}<r^{(m)}(t)^2>_t=\frac{1}{V}\sum_{m=1}^{N_t}\frac{1}{2}\lambda_m \tag{23}$$

As proved in Bergmann, M. ,2004

$$\frac{1}{T}\int_T r^{(m)}(t)^2 dt = \lambda_m \tag{24}$$

That is to say, the number of truncation N_{POD} is decided by the relative average mean fluctuation energy that the user decided. For example, the number of truncation $N_{POD}=4$ for 2D model Re=100 means the 4 first modes can represent the original fluid by conserving 99% of fluctuation energy or losing 1% of fluctuation energy. Notice that the mean average fluid energy has already been subtracted by equation 9 so that the eigen values represent the fluctuation energy rather than the energy for the whole velocity field.

2.4 Error of POD

Along with the relative average mean fluctuation energy, another criteria for the number of truncation is the difference between the original velocity field and truncated one called error of POD defined below:

$$\epsilon = \sqrt{\sum_{i=1}^{N_t}\sum_{I=1}^{node}\frac{\left(\boldsymbol{U}(I,t_i)-\boldsymbol{U}(I,t_i)_{truncated}\right)^2}{\left(\boldsymbol{U}(I,t_i)\right)^2}} \tag{25}$$

3 Reduced order model

The airship cruise speed is 28 m/s which is far less than Mach number 0.3, so the fluid can be considered as incompressible.The POD method will be applied to Navier-Stokes (NS) equation in order to modify Partial Differential Equation (PDE) to Ordinary Differential Equation (ODE) which makes the NS equation possible to solve.

3.1 POD for Navier-Stokes (PDE to ODE)

The Navier-Stokes equation for incompressible flows:

$$\frac{D\boldsymbol{U}}{Dt} = -\nabla P + \frac{1}{Re}\Delta\boldsymbol{U} \qquad where \frac{D}{Dt} = \frac{\partial}{\partial t} + \boldsymbol{U}\nabla \tag{26}$$

$$\nabla\boldsymbol{U} = 0 \tag{27}$$

The non-dimensional variable:

$$\boldsymbol{U} = \frac{\boldsymbol{u}}{V}, \boldsymbol{X} = \frac{\boldsymbol{x}}{L}, T_{period} = \frac{L}{V}, t = \frac{time}{T_{period}}, P = \frac{p}{\rho V^2}, Re = \frac{LV}{\nu}, \nu = \frac{\mu}{\rho} \tag{28}$$

Insert equation 7 of non-dimension formula to equation 26:

$$\frac{da^{(i)}(t)}{dt} + \sum_{m=1,n=1}^{N_{POD}} a^{(m)}(t)\,a^{(n)}(t)\left(\boldsymbol{\phi}^{(i)},(\boldsymbol{\phi}^{(n)}\bullet\boldsymbol{\nabla})\boldsymbol{\phi}^{(m)}\right)_\Omega = -\left(\nabla\ P,\boldsymbol{\phi}^{(i)}\right) + \frac{1}{Re}\sum_{m=1}^{N_{POD}} a^{(m)}(t)\,(\boldsymbol{\phi}^{(i)},\Delta\boldsymbol{\phi}^{(m)})_\Omega$$

$$\left(\boldsymbol{\phi}^{(i)},\Delta\boldsymbol{\phi}^{(m)}\right)_\Omega \equiv\ l_{im}, \qquad \left(\boldsymbol{\phi}^{(i)},\left(\boldsymbol{\phi}^{(n)}\bullet\boldsymbol{\nabla}\right)\boldsymbol{\phi}^{(m)}\right)_\Omega \equiv\ q_{inm} \tag{29}$$

where $i =\ 1,2,3,\ldots,\ N_{POD}$ The result shows the same formula from John, T. et al.(2010), which is called dynamical system(Noack, B.R. et al.,2003).

3.2 Viscous term

The viscous term $(\boldsymbol{\phi}^{(i)},\Delta\boldsymbol{\phi}^{(m)})_\Omega$ is noted l_{im} whose essential part is Laplacian :

$$\frac{\partial^2{\phi_x}^{(m)}}{\partial x^2} + \frac{\partial^2{\phi_x}^{(m)}}{\partial y^2} + \frac{\partial^2{\phi_x}^{(m)}}{\partial z^2}$$

Noack, B.R. et al.(2003) listed their explanation about l_{im} : the matrix of frequency and growth rate. For example the dynamical system of the flow around cylinder for the first 8 modes can represent as :

$$\begin{aligned}\frac{da^{(i)}(t)}{dt} &= \sigma_i\ a^{(i)}(t) - \frac{i+1}{2}\omega\ a^{(i+1)}(t) + h_i\\ \frac{da^{(i+1)}(t)}{dt} &= \sigma_i\ a^{(i+1)}(t) + \frac{i+1}{2}\omega\ a^{(i)}(t) + h_{i+1}\end{aligned} \tag{30}$$

where $h_i = \sum_{n=1}^{8} \sum_{m=1}^{8} q_{inm} a^{(n)}(t)\, a^{(m)}(t), \qquad i = 1, 3, 5, 7$

The Viscous term Matrix l is:

$$l = \begin{bmatrix} l_1 & 0 & 0 \\ 0 & \dots & 0 \\ 0 & 0 & l_4 \end{bmatrix} \qquad l_i = \begin{bmatrix} \sigma_i & -i\omega_r \\ +i\omega_r & \sigma_i \end{bmatrix} \tag{31}$$

where growth rate $\omega = 2\pi f = 2\pi \frac{St\, U_0}{D}$, $\omega_r = \omega Re$, f vortex shedding frequency ,St Strouhal number, D characteristic length. So that there are two solutions for l : one is solved by calculating the Laplacian of eigenvectors; the second is solved by calculating matrix l directly as the frequencies are known for different Re. The advantage of the first solution is that the method could be applied to different objects not only for cylinder and the frequencies and growth rate are not obligated to be known before. But the disadvantage is that the Laplacian of eigenvectors is not easy to calculate especially for the non-structured mesh. That's why the second method is more reasonable to adopt: with only limited number,the ODE could obtain the whole velocity field in a short time.

3.3 Convection term

The convection term $\left(\boldsymbol{\phi}^{(i)}, (\boldsymbol{\phi}^{(n)} \bullet \nabla)\boldsymbol{\phi}^{(m)}\right)_{\Omega}$ will cause the phase shift and differences of amplitude between one pair of coefficient like $a^{(1)}(t)a^{(2)}(t)$. Actually if the N_{POD} is large enough, there would be no difference of amplitude for the flow around cylinder as it is perfectly symmetry. This term could be calculated by gradient of eigenvectors. The same difficulty with viscous term is the complexity of non-structured mesh. But fortunately in the case of cylinder, comparing to the viscous term, the convection term is small enough to be neglected.

3.4 Pressure term

The pressure term is not easy to express by the combination of eigenfunctions. The previous researchers like B.Galletti et al.(2003) used linear model of the relevant projection term. But based on the research of Noack, B.R. et al.(2003), they pointed out that for the case of flow around cylinder, there is not too much effect for the result without pressure term.

3.5 Turbulence term

The different turbulence model like K- SST will create the complexity of this algorithm. The turbulence term would be a supplementary term. In this paper, the hypothesis of laminar is adopted.

3.6 Prediction by using POD reduced order model

One of the possible mission for POD reduced order model is prediction, that is to say, based on the hypothesis that the eigenvectors of Re=100 and Re=200 are the same, the POD reduced order model may predict the velocity field of Re=200 by using the information of Re=100 . And it can help to save time for the simulation and provides the possibilities to simulate in real-time. The methodology is listed below for an example of flow around cylinder seen in fig: In section 4, the experiment is conducted for the first attempt.

4 Adaptation for a cylinder

The 2D model with incoming lateral wind called 2D lateral airship is modeled as a cylinder.Two different case Re=100 and Re=200 will be detailed in this section. The mesh type of O-Mesh structured hexahedral divided into 9 blocks, where the zone around cylinder is cut by 4 contains 94196 points, 46780 cells. The velocity field and pressure field are cell-centered. The boundary condition is 1 m/s velocity inlet and 0 pascal pressure outlet. $\rho = 1kg/m^3, \nu = 0.01m^2/s, U_0 = 1m$ whose correspondent physic explanation is a cylinder of 1 m diameter in air of 1 m/s velocity. $\Delta T = 0.005s$. To reach the established regime, the write Interval is 1000 from 0s to 400s which means the data saves in every 5s. From 400s to 420s, the write Interval is 10 so that the data can save in every 0.05s to capture the details. The result needed for POD are saved in file U for velocity field, file p for pressure field for each write interval (0.05s) from 400s to 420s.

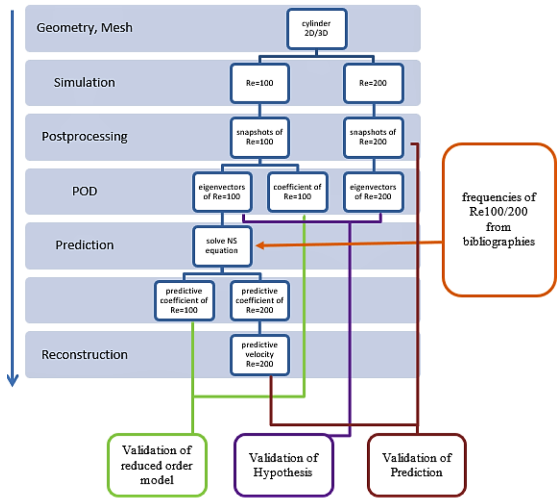

Fig. 2. methodology of prediction

4.1 Number of samples for cylinder wake

It is shown in Section 2 that the more samples can approach more to the high fidelity model. But due to the capacity of the computer, it is better to choose a reasonable number to be large enough to generalize all the features. One criteria for for the fluid dynamics around a cylinder is frequency. When the number of Reynolds is more than 40, the Von Karman vortex appears which creates the periodic flow(Demartino and Ricciardelli, 2017). When the Re=100, Strouhal number $St = \frac{fD}{U_0} = \frac{D}{TU_0}$ is between 0.1 and 0.2 where T is the period of Von Karman. As the period is 5s after simple calculation, with $\Delta T = 0.005$ and write interval 10, it's better to choose the samples more than 100 to extract at least one period. Empirically, 300 samples with 3 periods of Von Karman can provide a convincible result as Bergmann M. (2004) used the 305 samples around 3 periods.

4.2 Normalization and orthogonality

To ensure the validity of the POD algorithm, after the calculation of eigenvectors, the normalization and orthogonality of these eigenvectors and coefficient can be tested following this formula:

$$a^{(m)}(t)\,a^{(n)}(t) = \delta_{mn} = \begin{cases} 0, ifm \neq n \\ 1, ifm = n \end{cases} \tag{32}$$

$$(\boldsymbol{\varphi}^{(m)}, \boldsymbol{\varphi}^{(n)}) = \frac{1}{N_t \lambda_m}(\boldsymbol{\phi}^{(m)}, \boldsymbol{\phi}^{(n)}) = \begin{cases} 0, ifm \neq n \\ 1, ifm = n \end{cases} \tag{33}$$

In this paper, both of them are validated, for example $(\boldsymbol{\varphi}^{(1)}, \boldsymbol{\varphi}^{(2)}) = 2.8796e^{-16} \approx 0$

4.3 Eigenvectors and eigenvalues

The eigenvector represents the eigen velocity field $\boldsymbol{\varphi}$.As the number of samples increases, the eigenmode becomes more and more symmetric which means that these eigenmodes capture the whole information for periodic flow where the choice of start time for the samples would not influence the form of eigenmode.By using scalar-POD, the fluctuation energy truncated is 99% for x direction, which decides to conserve first 4 eigenmodes. But meanwhile the number of mode should be the same in y direction and z direction so that it could not ensure the POD contains 99% fluctuation energy for the whole velocity field which is one of the disadvantages of scalar-POD. Figure 3 shows the comparison between the scalar-POD and POD, the POD is more similar to the flow of high fidelity model and also the reality as the zone near boundary is not influenced too much by the mesh. That is to say, it has less mesh noise. One reason for this different performance is that the scalar-POD calculates the correlation in a separate way, so that the velocity norm could not perform the best representative flow while each direction could be more precise and representative than POD method. The proof is that after checking the error of POD, the error of scalar-POD is less than POD seen in table 1 which means each subspace for each direction could capture more information than POD. But in order to choose the better reduced model without influence of mesh, the POD method is adopted.

The figure 4 shows the POD method, the fluctuation energy truncated is 99.99% with first 8 modes. By comparison the figure 5 from Noack et al.(2003), the POD is well conducted to 2D lateral model.

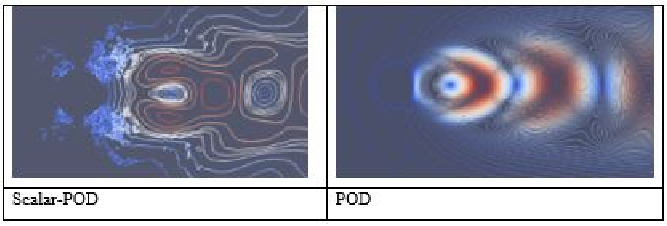

Fig. 3. Comparison of mode 1 velocity norm between scalar-POD and POD for Re 100

Table 1. Comparison of error(scalar-POD and POD)

Re 100	Scalar-POD	POD
ϵ	3.2163e-10	7.0761e-4

Table 2. Frequencies of 8 first modes

Re 100	mode 1,2	mode 3,4	mode 5,6	mode 7,8
frequency	0.157	0.325	0.457	0.625

It is interesting to find that the pair of eigenmode mode 1,2 or mode 3,4 have similar properties : the streamline, energy spectrum see in figure 6, frequency of coefficient in table 2.What's more,the frequency represents the frequency of vortex shedding,and the mode 3,4 is the double of frequency of mode 1,2. In the same time, the pair of eigenmode shows the property of interleaving similar but with the inverse direction which corresponds the mathematical expression of dynamical system in equation 30.

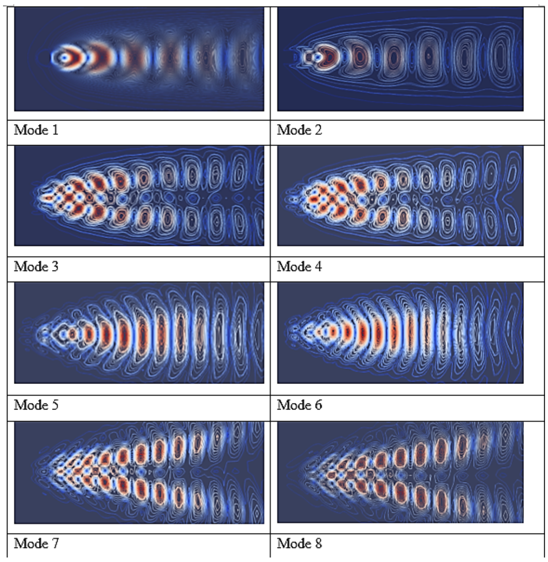

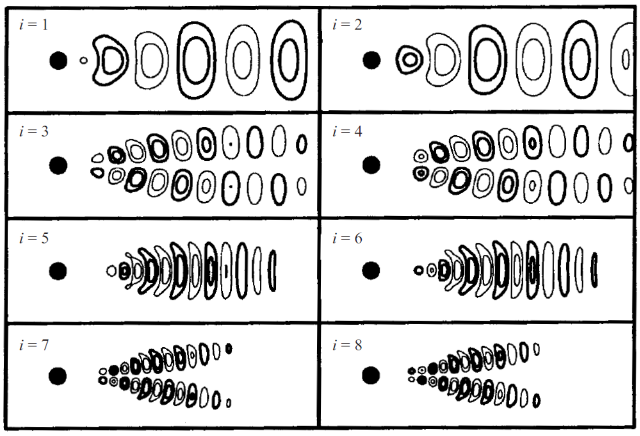

Fig. 4. Comparison of mode 1 velocity norm between scalar-POD and POD in Re 100

Fig. 5. Re=100 with 100 samples from Noack et al.(2003)

To validate the hypothesis of section 3.6, the eigenvectors of Re 100 should not vary too much from Re 200. In order to compare the first 8 modes with Re 100, the fluctuation energy chosen for Re 200 is 99.9%.

The table 3 shows the comparison of eigenvectors in Re 100 and Re 200.The more energy conserved, the less error it has between eigenvectors of Re100 and Re200. It is quite clear that the more energy conserved, the eigenvectors represent the real field better. But even though with 0.0001% of energy loss, the difference between of eigenvectors of Re 100 and Re 200 is still large. And the error varies with the choice of start time as the initial condition of Re 100 and Re 200 may not be the same, so that it could be a source of error.

4.4 Coefficient and reduced order model coefficient

The coefficient of POD is the $r^{(m)}(t_i) = \sqrt{N_t \lambda_m}\; b_m(t_i)$ in equation 19. After testing with 200 samples and 300 samples, the ellipse or circle with decentering from zero for $r^{(1)}(t_i)$ and $r^{(2)}(t_i)$ shows that it is not the best coherent structure with the reality. Because the sample selected cannot cover the complete period, it might cover 4/3 or 8/5 period so that the circle will shift from zero. A better choice for Re 100 is around 256 samples, 2 times of complete period and also integral times of other coefficients.

Figure 7 shows the first 8 mode reduced order model coefficient calculated by ODE with the comparison of simulation result.

Table 3. Eigenvectors(Re100/Re200) comparison

Case	Energy loss(Re100)	Energy loss(Re200)	ϵ
case1	0.03%	0.1%	283.36%
case2	0.03%	0.03%	46.61%
case3	0.0001%	0.0001%	32.61%

Table 4. Coefficient(full model/POD/ROM) comparison

model	full model	POD	ROM
$\epsilon(Re100)$	0%	0.070761%	0.55%
$\epsilon(Re200)$	0%	0.28%	1.57%

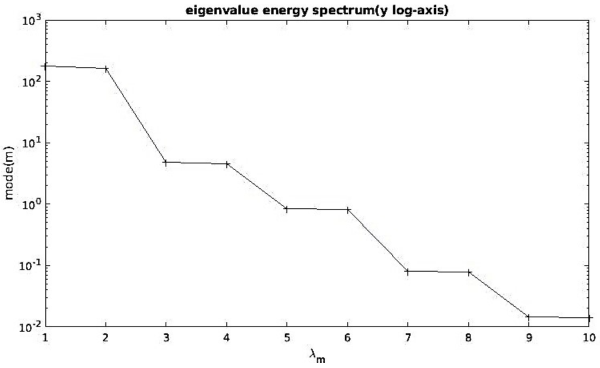

Fig. 6. Energy spectrum of 10 first mode for cylinder Re=100 with 256 samples POD(log)

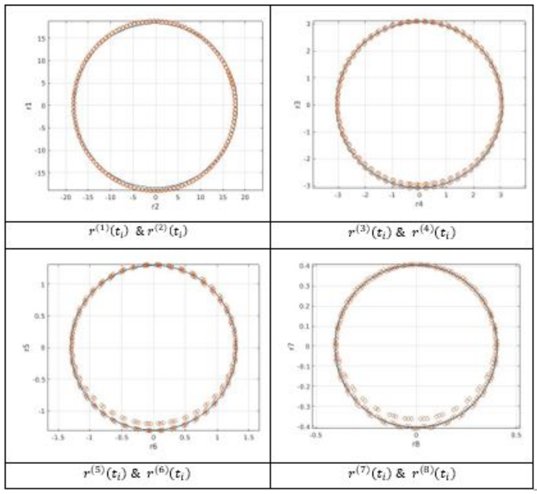

Fig. 7. Re 100 with 256 samples for simulation coefficient(points)and reduced order model coefficient(lines)

The differences appear more for the smaller eddies or higher mode because the amplitude of higher mode is quite small so that it is easier to be influence by the litter nuance.The experiment of Re 200 is conducted too. The comparison is shown is table 4.

4.5 Prediction from Re100 to Re200

As mentioned in section 3.6, the prediction is by using eigenvectors of Re 100 to solve ROM model in Re 200. But the error after reconstruction is from 11.5% to 15.13% with the shift sampling.The error is mainly due to the inequality of eigenvectors of Re100 and Re200 seen in table 3.

In conclusion,the reconstruction of the POD shows a good performance for not only Re 100 but also Re 200, so that the capability of information compression is well conducted by POD. Besides, the error of reduced order model coefficient shows a good construction of reduced order model.

5 Adaptation of prolate spheroid

After testing in 2D lateral model, the 3D lateral airship is modeled as a form of prolate spheroid seen in fig 9. The total number of node is 15632408, the simulation is validated by analyzing the frequency of lift coefficient.

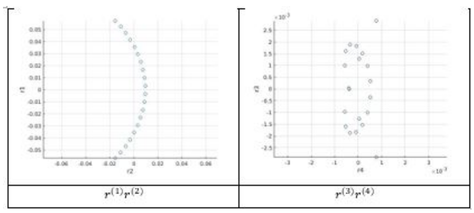

Fig. 8. Coefficient of 3D eigenvectors of prolate spheroid Re 100 for 20 samples

Inlet velocity 0.001 m/s,$\nu = 0.00001 m2/s$ Re=100.It is impossible for 200 sample to load 15632408 node number in MATLAB with the limited space. So that only 20 samples will be used in this section. The fluctuation energy truncated is 0.9999 so that the first 4 mode conserves. After reconstruction the error is 3.195e-5, it shows the good capability of conservation information of POD even though in 3D case with only 20 samples. The iso contour of the norm of velocity field is shown in figure 9 and its projections are shown in figure 10.

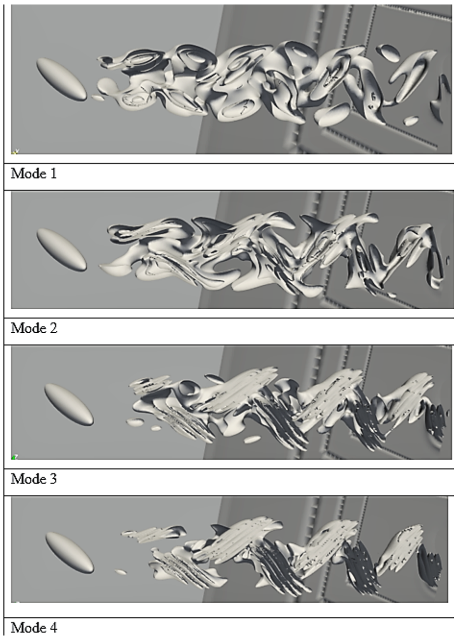

Fig. 9. Cross profile 3D eigenvectors of prolate spheroid Re 100 for 20 samples

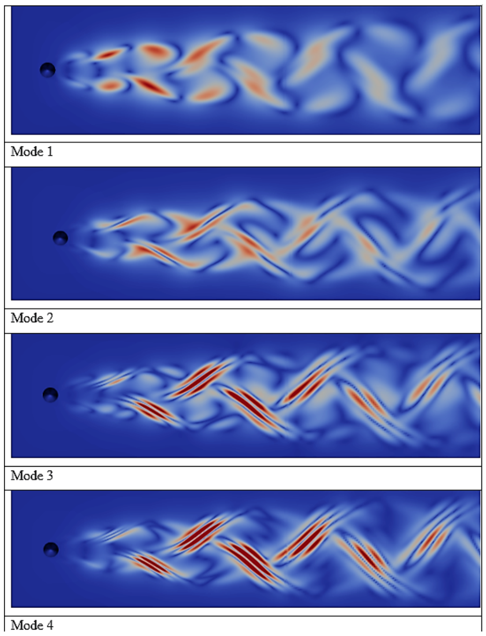

Fig. 10. Projection of 3D eigenvectors of prolate spheroid Re 100 for 20 samples

Only 20 samples could not capture all the information and keep the symmetry of eigenvectors.But the more number of sample it has, the more symmetry the eigenvectors could be.The figure 8 shows its coefficient but as the limited sample, it could not offer a precise result, so the ROM test is left for the future work.

6 Conclusion

The POD is a strong tool for compressing information and analyzing the properties of a fluid field. In this report, the interpolation method is well detailed and explains the difference between the various available methodologies by different researchers on POD. The comparison of the classical POD and snapshot POD is shown and the snapshot shows better performance for the consideration of large mesh. In section 4, it also shows the difference of the scalar-POD and POD, these result indicate that POD method is more coherent and less influenced by the mesh than scalar-POD, so that the POD snapshot is adopted to predict the flow from Re 100 to Re 200.

With the method of POD, the Navier-Stokes equation can be simplified into ODE. With the hypothesis of neglecting convection and pressure term, the simplified viscous term based on frequency of vortex shedding can represent the reduced order model created for 2D lateral model. With the validation of the error after POD, the result shows that POD conserves information well as it only has 7e-4 error between the original field and reconstruction field.

After the test of reduced order model coefficient created with growth rate 0, the hypothesis of neglecting convection, pressure term and simplification of viscous term can be validated as the error is only around 5e-3.

After the validation of 2D lateral model, the 3D lateral airship model: prolate spheroid is tested with 20 samples. The result shows a better coherence with the understanding of 2D model but due to the limitation of the space, the number of samples is not sufficient enough but this could be accomplished in the future.

In conclusion, this report provides a successful method of proper orthogonal decomposition for velocity field in 2D which is coherent with the bibliographies and create reduced order model 2D successfully to reconstruct the velocity field. Besides, the application of 3D gives a good inspiration of reduced order model for 3D lateral airship by modifying the parameters in the matrix l. Finally the prediction from Re100 to Re200 contains around 12% error mainly due to the large difference between the eigenvectors from Re100 and Re200.

References

1. Amsallem, D., Cortial, J and Farhat, C.,2010. Towards real-time computational-fluid-dynamics-based aeroelastic computations using a database of reduced-order information. AIAA journal, 48(9), pp.2029-2037.
2. Atwell J.A.,2000. Proper Orthogonal Decomposition for Reduced Order Control of Partial Differential Equations. PhD dissertation, Virginia Tech.
3. Atwell J.A. and King B.B.,1999. Reduced order controllers for spartially distributed systems via Proper Orthogonal Decomposition. Technique report, ICAM 99-07-01, Virginia Tech.

4. Barone, M.F., Kalashnikova, I., Brake, M.R. and Segalman, D.J.,2009. Reduced order modeling of fluid/structure interaction. Sandia National Laboratories Report, SAND No, 7189, pp.44-72.
5. Bergmann, M. ,2004. Optimisation arodynamique pat rduction de modle POD et contrle optimal.application au sillage laminaire d'un cylindre circulaire. Chapitre 4, PhD dissertation, Institut national polytechnique de lorraine,in french.
6. Braud, C., Heitz, D., Arroyo, G., Perret, L., Delville, J. and Bonnet, J.P., 2004. Low-dimensional analysis, using POD, for two mixing layer-wake interactions. International journal of heat and fluid flow,25(3), pp.351-363.
7. Brunton, S.L. and Noack, B.R.,2015. Closed-loop turbulence control: progress and challenges. Applied Mechanics Reviews, 67(5), p.050801.
8. Chen, H., Reuss, D.L., Hung, D.L. and Stick, V.,2013. A practical guide for using proper orthogonal decomposition in engine research. International Journal of Engine Research, 14(4), pp.307-319.
9. Cordier, L. and Bergmann, M. 2003a. Lecture Series 2003-04 on post-processing of experimental and numerical data: Proper orthogonal decomposition: an overview, Von Karman Institute for Fluid Dynamics.
10. Cordier, L. and Bergmann, M. 2003b. Lecture Series 2003-04 on post-processing of experimental and numerical data: Two typical applications of POD: coherent structures education and reduced order modelling, Von Karman Institute for Fluid Dynamics
11. Courant R. and Hilbert D.,1953. Methods of mathematical physics, 1. John Wiley and Sons, New-York.
12. Demartino, C. and Ricciardelli, F., 2017. Aerodynamics of nominally circular cylinders: A review of experimental results for Civil Engineering applications. Engineering Structures, 137, pp.76-114.
13. Eisenberg, M.A. and Malvern, L.E.,1973. On the finite element integration in natural co-ordinates. International Journal for Numerical Methods in Engineering, 7(4), pp.574-575.
14. Galletti, B., Bruneau, C.H., Zannetti, L. and Iollo, A., 2004. Low-order modelling of laminar flow regimes past a confined square cylinder. Journal of Fluid Mechanics, 503, pp.161-170.
15. Holmes, P., Lumley J.L. and Berkooz G.,1996. Turbulence, Coherent Structures, Dynamical Systems and Symmetry. Cambridge Monographs on Mechanics.
16. John,T., Guay, M., Hariharan, N. and Naranayan, S., 2010. POD-based observer for estimation in Navier-Stokes flow. Computer & Chemical engineering, 34(6), pp.965-975.
17. Liberge, E. and Hamdouni, A., 2010. Reduced order modelling method via proper orthogonal decomposition (POD) for flow around an oscillating cylinder. Journal of fluids and structures, 26(2), pp.292-311.
18. Lieu, T. and Farhat, C.,2007. Adaptatioon of Aeroelastic Reduced-Order Models and Application to an F-16 Configuration. AIAA Journal, 45, pp.1244-1257.
19. Lumley, J.,1967. The structure of inhomogeneous turbulence flow. In: Yaglom, A., Tararsky(Eds.), Atmospheric Turbulence and Radio Wave Propagation. Nauka Press, Moscow, pp.166-178.
20. Morgan, K. and Peraire, J.,1998. Unstructured grid finite-element methods for fluid mechanics. Reports on Progress in Physics, 61(6), p.569
21. Noack, B.R., Afanasiev, K., MORZYSKI, M., Tadmor, G. and Thiele, F., 2003. A hierarchy of low-dimensional models for the transient and post-transient cylinder wake. Journal of Fluid Mechanics, 497, pp.335-363.
22. Noack, B.R., Morzynski, M. and Tadmor, G. eds., 2011. Reduced-order modelling for flow control (Vol. 528). Springer Science & Business Media.
23. Porion, F.,2016. Karhunen Love expansion and distribution of non-Gaussian process maximum. Probabilistic Engineering Mechanics, 43, pp.85-90.
24. Riesz F. and Nagy B.S.,1955. Functional Analysis. Ungar,N.Y.
25. Sirovich, L.,1987. Turbulence and the dynamics of coherent structures, part i: coherent structures; part ii: symmetries and transformations; part iii: dynamics and scaling. Quarterly of Applied Mathematics, 45(3), 561-590.
26. Turk, M. and Pentland, A.,1991. Eigenfaces for recognition. Journal of cognitive neuroscience, 3(1), pp. 71-86.
27. Zienkiewicz, O.C., Taylor, R.L., 1977. The finite element method (Vol.3 Fluid dynamics) .London: McGraw-hill.